Characterization of misfit dislocations in Si quantum well structures enabled by STEM based aberration correction

Philip E. Batson*, Maureen J. Lagos

Institute for Advanced Materials, Devices and Nanotechnology, Rutgers University, Piscataway, NJ 08854, United States

ABSTRACT

The success of aberration correction techniques at the end of the 20th century came at a time of increasing need for atomic resolution imaging to better understand known structural defects that influence semiconductor device operation, and to advance the search for new structures and behavior that will form the basis for devices in the future. With this in mind, it is a pleasure to recognize the contributions of Ondrej Krivanek to the success of aberration correction techniques, and his extension of aberration techniques to EELS equipment that further promises to unite structural studies with characterization of behavior from meV to keV energies in the STEM.

© 2017 Published by Elsevier B.V.

In 2000, I reported imaging and spectroscopy results on single misfit dislocations which decorate the electrical interface between strained Si quantum wells, and the GeSi alloy in $Ge_xSi_{(1-x)}$ structures [1,2]. These misfit structures are known to occur when the Si thick- ness exceeds the Matthews-Blakeslee value for pseudomorphic growth, creating sufficient strain to favor injection of 60° dislocations, [3] which then dissociate, to create 30° (P30) and 90° (P90) partial dislocations separated by an intrinsic stacking fault (ISF). In earlier experimental work, the misfit structure had been suspected to contribute to limited electron mobility in strained hetero-structures, [4] and to luminescence in heavily deformed silicon, possibly enabled by electrically active states within 0.1 eV of the conduction band (CB) minimum [5,6]. TEM and luminescence studies confirmed optical activity near the defects, but the atomic structure had not been determined [7–12].

Theoretical work with likely core structures also had not found strong evidence for optical activity at either the stacking fault, [13–15] or at straight partial dislocations bounding the fault, [16–18] largely because dislocation cores appear to reconstruct to clear the gap of electronic states. Theoretical studies of P90 structures also found that they are likely to reconstruct to lower their total energy. [19, 20] And, finally, there had also been some theoretical evidence for shallow valence band states. [21]

In the 2000 work, spatially resolved Electron Energy Loss Spectroscopy (EELS) of dissociated misfit dislocations in a strained Si quantum well imbedded in $Ge_{0.35}Si_{0.65}$ revealed the local conduction band at the P30 dislocation, the ISF, the P90 dislocation, and in the strained regions near the defect. Atomic column positions in the [110] projection, and the spatial location for the spectral results were obtained using Annular Dark Field (ADF) imaging in the STEM using a 2.2°A probe at 120 keV. Fig. 1 summarizes the HAADF imaging result, where we clearly can identify the bounding partial dislocations, a 10 unit Intrinsic Stacking Fault, (ISF) and, otherwise continuous bonding of the Si Quantum well (at the bottom) and the $Ge_{0.35}Si_{0.65}$ substrate (at the top).

Also in the 2000 work, and summarized in Fig. 2, I obtained spatially resolved EELS point spectra from several unique areas-the two partial dislocations, the ISF and the bulk GeSi alloy. Strong features include a splitting of 101 eV L_1 conduction band peak into two contributions for the ISF and P30 structures. At the P90 partial, however, the 2p L_1 shape strongly resembles the bulk relaxed alloy scattering, except for a broadening of the onset downwards by about 0.3 eV, a feature that is in common with the P30 partial. Finally, the absolute value of the edge onset is also found to be sensitive to the local strain, as shown for regions that are in tension and in compression in the image. These structures can be understood by reference to simple distortions and broken bonding symmetry. For instance the splitting of the L_1 band results from the 180° rotation of the lattice about the [111] direction in the ISF. In that configuration, the third neighbor atoms are closer together than in the bulk, with a concurrent strengthening of their interac-
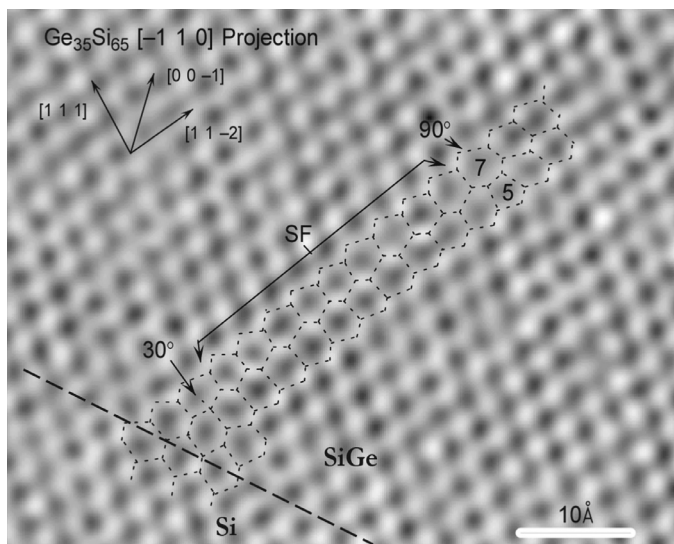
Fig. 1. Using the 2.2 ˚A probe, the misfit dislocation can be imaged and largely modeled using simple structures. This image is adapted from Fig. 3 of [35]. In this image, the Si quantum well is located on the bottom, below the dashed line. The misfit dislocation contains a P30 partial dislocation, an intrinsic stacking fault (ISF), and a P90 partial dislocation. In this simple model, the P30 dislocation contains a single column, while the P90 dislocation is modeled with 5,7-fold rings.
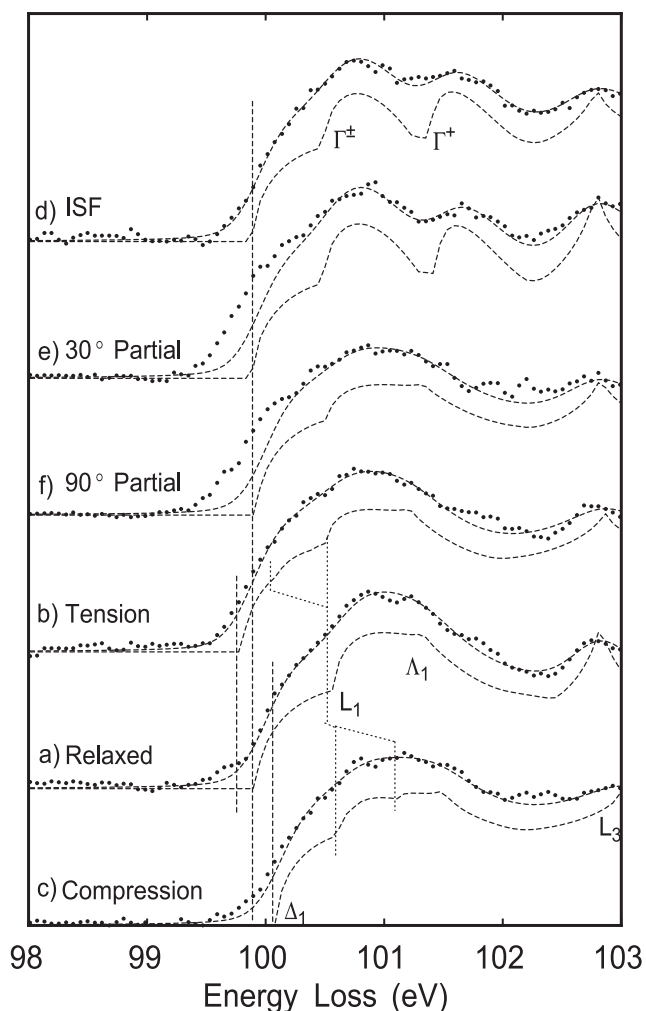
Fig. 2. Six EELS 2p core level spectra obtained from several areas, as labeled. The various differences are discussed in the main text. Reproduced from [2].

tion, driving a stronger orbital hybridization and splitting of the L_1 peak. It is therefore a puzzle as to why the P90 dislocation does not show a similar splitting.

A new model for the P90 has been suggested by Bennetto, Nunes and Vanderbilt. [19,20] based on energy considerations. This introduces a Double Period (DP90) reconstruction at the core through the addition of kinks in the [1 1 −2] direction within the plane of the ISF. A view of this model, overlaying image intensity is shown in Fig. 3 for the "qudn" variant of their model. This model has the interesting property that, if viewed in the [1 1 0] direction at 2.2 ˚A spatial resolution, the four core atom columns would not be resolved, but would appear as a single symmetric blob.

It was therefore with high anticipation that, in 1998–1999, I was watching the work of Ondrej Krivanek and Niklas Dellby in Cambridge, who were aiming to improve the spatial resolution of an existing VG Microscopes STEM, through the use of electron optics to remove limitations of spherical aberration in the aging instrument. They successfully demonstrated to my satisfaction that they had mastered this difficult task, that had eluded many previous researchers during the first 50 years of electron microscopy [22]. And so in the fall of 1998, with funding from IBM, we decided to insert a simple quadrupole-octupole corrector into the column of the IBM VG machine to see where it would take us. My dream, of course, was that the four column P90 partial dislocation structure would become viewable in this work.

Fig. 4 shows a summary of the mechanical changes which were needed to allow integration of the corrector with the VG HB501 STEM. Besides the obvious changes, there were also many difficulties related to the large enhancement of performance that we were trying to obtain. The VG machine, of course was originally delivered with a probe size of about 0.5 nm. During the 17 years of operation before the introduction to aberration correction, it received a high resolution polepiece to improve its intrinsic spherical aberration. Its acceleration voltage was raised to 120 kV from 100 kV to improve beam current and lower the effective probe size to about 2.2 ˚A. Its magnetic spectrometer was replaced with a high resolution Wien filter located at high voltage to produce an EELS energy axis that could be calibrated to about 20 meV accuracy over 1 keV [23]. And its oil diffusion pump was replaced with a high capacity ion pump to improve the quality of the vacuum in and around the specimen. Even so, our first results were severely limited by AC interference, largely from the VG electronics that were never intended for use with an Angstrom level instrument [24]. It should be noted that since it's invention in the late 1930′s, electron microscopy has been under continuous development aimed at higher performance, so it would seem that the technology which makes it possible, and the associated physical science that it reveals, should have been well explored in 1998. But it took the electronics revolution of the 1990′s to produce affordable computation to design complex multipole lens systems. This capability was also ideally positioned to allow the fabrication of inexpensive current regulating circuits to control and stabilize many sets of current supplies with parts per million stabilities. Thus for many years aberration correction theory was well developed in principle, but in practice no corrector system had managed surmount the barriers presented by noisy electronics, poor control over the needed mechanical tolerances, lack of computer aided design tools, and the lack of digital techniques for control and optimization of performance.

In 2000–2001, Ondrej and Niklas delivered the performance that we all hoped for. The effort paid off and we produced a sub-angstrom probe size for the first time [25]. And as a result we are now experiencing a swift development of new microscopy techniques, based on our improved capability to control the lateral properties of kilovolt electron beams, even to the Angstrom level, allowing us to locate, identify and discover how atoms behave, singly and in small groups, imbedded within bulk materials
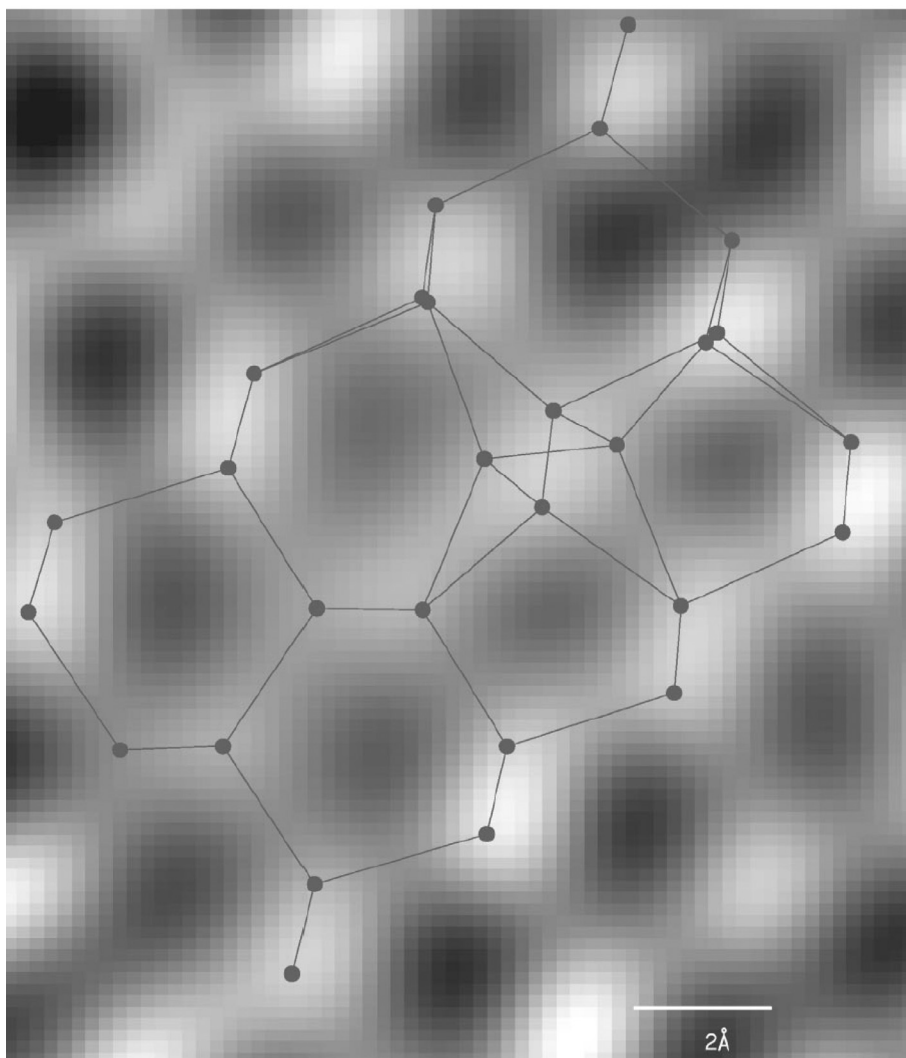
Fig. 3. Overlay of Double Period "qudn" model structure [19, 20]. The structure requires [1 1 −2] kinks in the structure for every other [1 −1 0] plane extending into the plane of the material. The resulting structure has four atom columns, spaced about 1 °A apart within the core of the P90 dislocation.

[26]. This was a singular achievement and one has to step back for a moment and acknowledge the drive and dedication to practical design goals that Ondrej summoned to this task.

Fig. 5 summarizes the improvement in imaging performance achieved with the first system. Si Dumbbells are obvious and we estimated a probe size from single atom images to be as small as 0.75 °A. This result required several months of effort beyond the initial installation to clean up electrical ground loops, floor vibration and acoustic interference, in addition to existing AC magnetic shielding.

Fig. 6 shows the improvement in imaging of the P90 partial dislocation. Dumbbells are clearly identified, and atom column positions allow us to orient to the direction of the dumbbells and to determine those positions down to a little over 1 °A. In about 1/3–1/2 of the images that we obtain, the core structure clearly consists of four separate columns in a roughly square pattern. In Fig. 6, we show column locations for one of the several structures obtained by theory [27]. We find also that the P30 structure is identical to that obtained without the corrector.

In Fig. 7 we compare a frame which shows the four column motif, with one which does not. These were obtained using a 0.2 sec frame time, in sequence. Thus this core structure is not-stable for long periods of time, at least when viewed at 120 keV and using 100 pA currents. However, this is not a surprise, because we knew from the theory that several motifs exist and that they are only fractions of an electron volt different in formation energy. Thus, we suspect that the structure should explore several of these motifs during the observation. It must also be realized that the existence of the square motif in the image does not necessarily prove the existence of the DP structure, since multi-slice calculations show that a single kink in an otherwise simple 5,7-fold ring structure can show the square motif if the kink is at or within one or two layers of the entrance surface for the electron beam. If such a kink is deeper than that, however, the effect of a single kink on the image is small.

At Rutgers, we have been very interested in an instrument that can obtain EELS intensity at high energy resolution, down to and into the phonon regime. The problems that we would like to address include photonic behavior of sub-wavelength sized metal and dielectric objects; Surface Enhanced Raman Scattering and molecular sensing [28,29]; and plasmonic enhancement for photovoltaics [30]. We believe that many behaviors that are now the subject of interest in the photonics and plasmonics community will also be valuable at phonon energies.

Fig. 8 shows the new Nion UltraSTEM with the Hermes monochromator at Rutgers. As we learned with the first Nion cor-
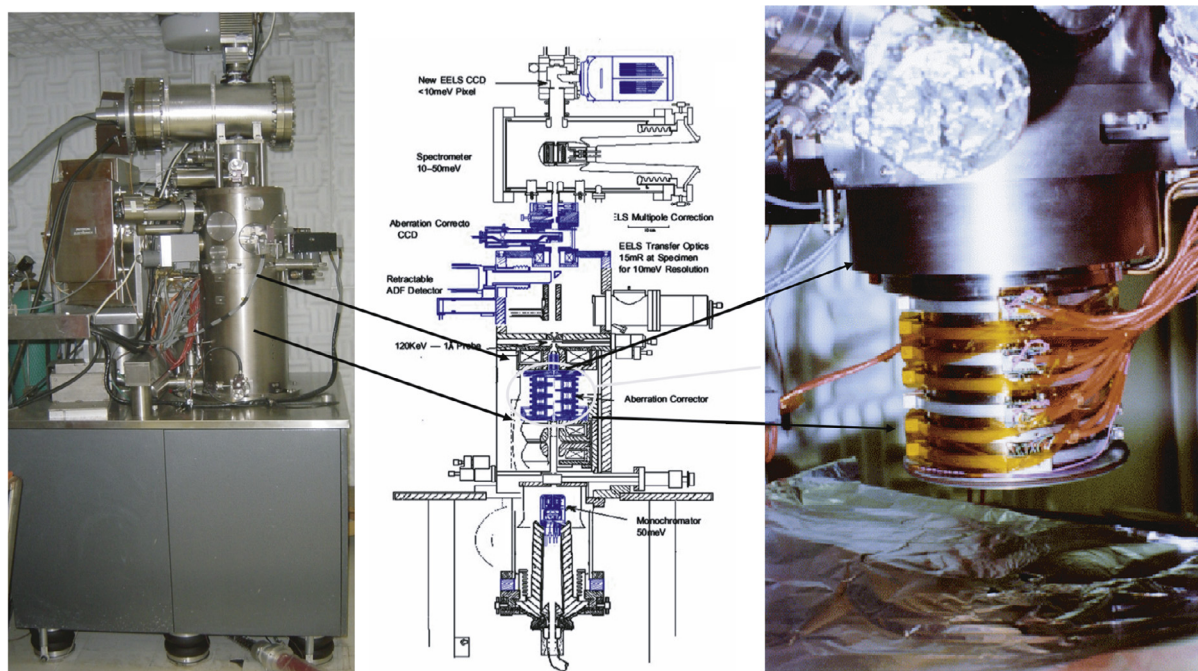
Fig. 4. The VG Microscopes HB501, delivered in 1983, was subsequently configured for 120 kV operation with high resolution EELS [36]. The line drawing shows modifications needed for the new aberration optics, between the objective and condenser lenses. At the top, optics at the entrance to the spectrometer needed to be rebuilt to make room for the Ronchigram camera. On the right, is a photo of the 35 lens corrector mounted under the VG objective lens, during installation.
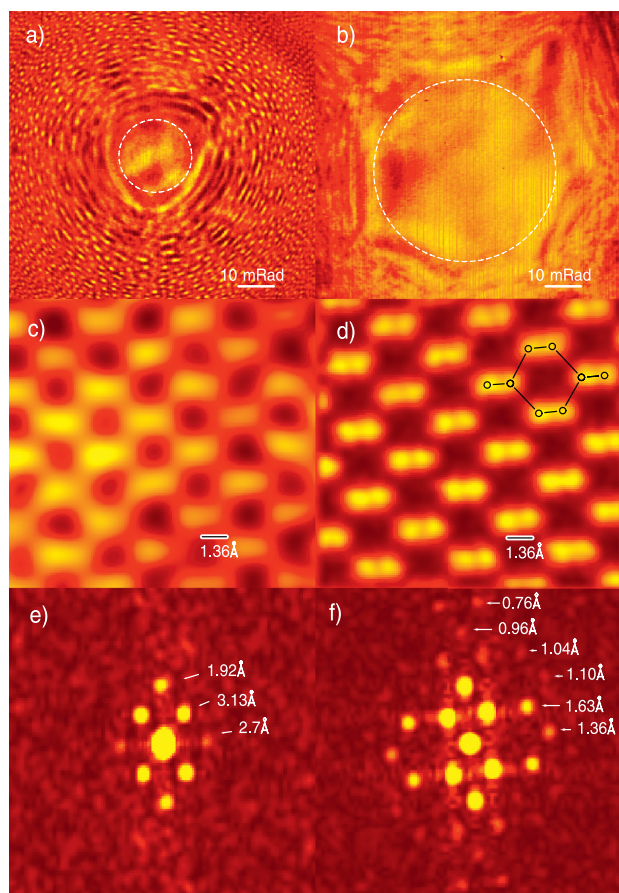

Fig. 5. Comparison of imaging performance, with correction turned off (left), and correction turned on (right), after installation of the Nion 3rd order aberration corrector in the IBM VG HB501 STEM. Dumbbells are easily resolved with the corrector and FFT spots are available beyond 1 Å. Reproduced from [25].
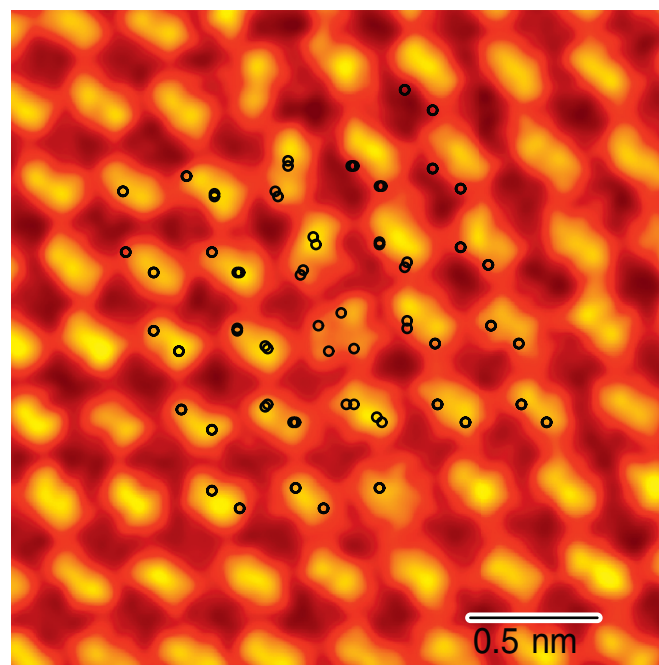
Fig. 6. Image of a P90 partial dislocation with aberration correction, with an overlay of positions predicted by theory for the Double Period (DP) reconstruction of the P90 core [27].

rector, the room environment is very important to the ultimate performance of the system. Floor vibration velocity is about 1 μ per sec; AC magnetic fields are about 4 micro-gauss RMS at 30 Hz, and lower at higher frequencies; thermal variations are within 0.1 °C for many hours or days; and acoustic interference is below 20 dbA. Currently available machines may not require such stringent envi- ronmental conditions with the use of a removable canopy. However, as Fig. 8 shows, this instrument does not have
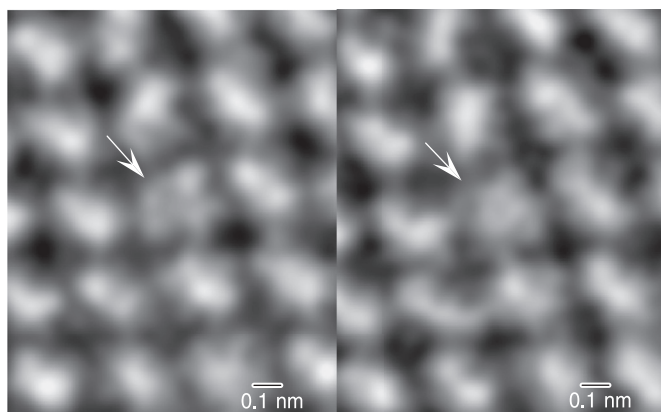
**Fig. 7.** Comparison of two images that show movement of the DP core structure from one frame to another.

this protection and so we were very careful with the room in compensation. The new instrument demonstrates sub-10 meV resolution routinely. We also show in Fig. 8 an example from BN, where we believe we have captured polaritonic behavior, or coupling of the BN surface phonon with photons in the vacuum above and below the planar sample. This is evident in the 14 meV splitting, which results from symmetric and anti-symmetric coupling of phonon polariton modes across the thickness of the BN thin film.

In Fig. 9, we model the BN phonon polariton scattering, for a 20 nm thick flake, using inelastic scattering theory. We used both the non-retarded expressions from Ritchie [31], and retarded results for uniaxial crystals from Chen [32], and a parameterized set

of optical constants from Geick, et al. [33]. The results capture behavior from both upper and lower Reststrahlen bands, which are driven by c-axis and a,b axis dielectric behavior respectively. Although, in this exercise we are really only seeking to verify that the result is reasonable, we find remarkable agreement with the experiment. BN has a very rich behavior, due to its anisotropic dielectric response, and so we are looking forward to further exploration in this and other anisotropic materials.

The second part of this project on misfit dislocation behavior, is to better understand the EELS structure at the Si 2p core excitation for the different core structures. As shown above in Fig. 2, there are several distinctive structures that we believe are related to the whole P30-ISF-P90 misfit dislocation. We believe that optical activity is likely to be associated with the displaced thresholds of the edges at the P30 and P90 partial dislocations. However, with the available energy resolution of about 280 meV using the Wien Filter spectrometer on the VG machine, we cannot tell if the apparent shift in the conduction band is a real shift driven by strain, or if it is, perhaps, an impurity state which is distinct from the conduction band. We will need a better EELS performance for that.

In Fig. 10 we show the EELS performance using the new Hermes monochromator to obtain a high resolution 2p core loss in Si. Briefly, the Hermes spectrometer is potentially a very high resolution device. We have on several occasions measured the zero loss FWHM to be 7.5 meV. However, for the Si core loss measurement, the line width limited by the physics of the core decay processes is of order 100 meV, thus we will not need the very highest resolution capability for this measurement. In addition, we also need to be aware that the Nion system disperses in energy using magnetic elements at ground potential, operating on the keV electrons
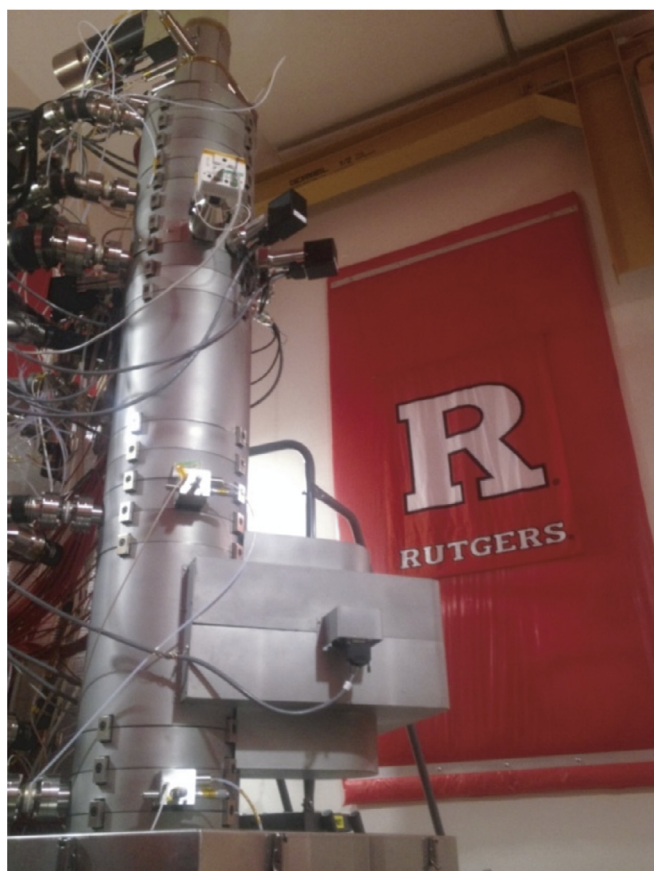
Fig. 8. Overview of the new Nion UltraSTEM with Hermes monochromator and high resolution spectrometer. The EELS low energy performance is summarized.
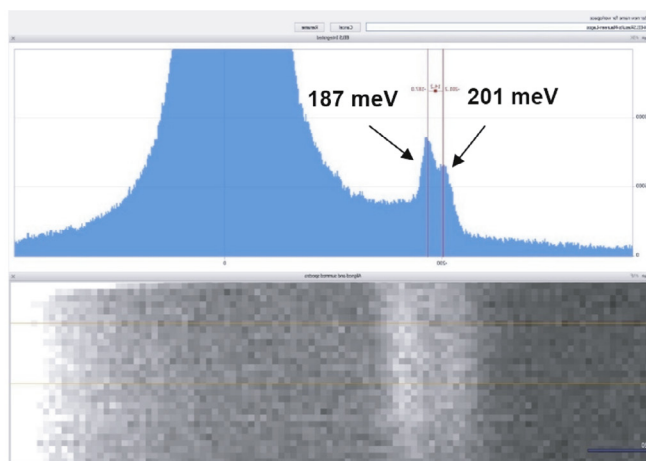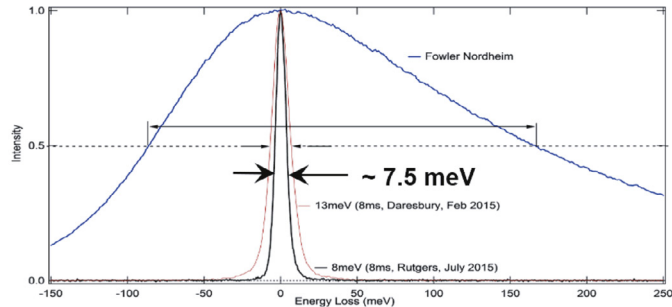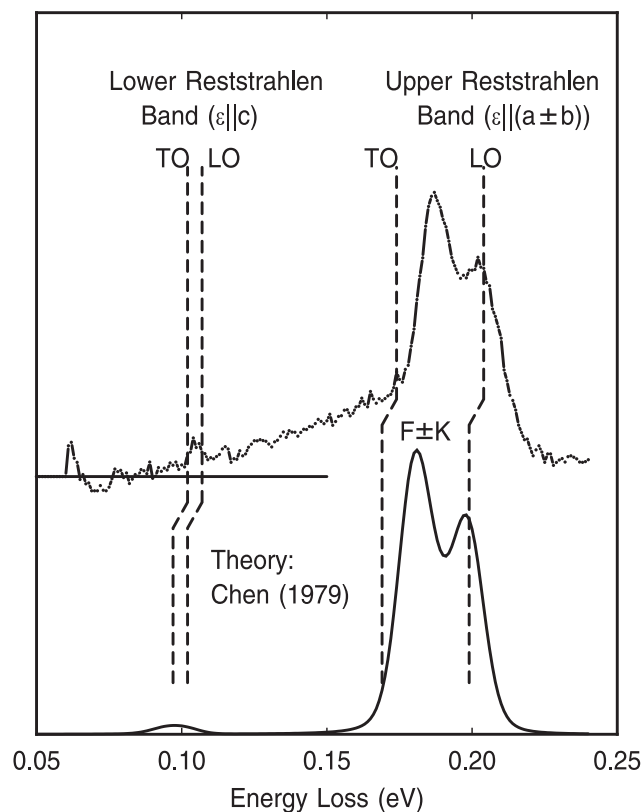
Fig. 9. Comparison of the experimental BN phonon polariton splitting with theoretical results. The thickness was adjusted to 20 nm to match the shape of the experimental data. Angles were integrated to 13nm⁻¹ or about 10mR at 60 KeV.

directly. Thus, while the system has a very high energy resolution, day to day minor changes in the magnetic configuration of the magnetic dispersion elements produce errors that are possibly in the 10's to 100's of meV in the absolute measurement at core edge energies. The Wien filter on the VG machine, floating at the gun potential, obtains high resolution by decelerating electrons to about 100 eV Thus, the center pass energy of the filter determines the absolute value of the center of the energy loss spectrum. In the VG machine, then, a reproducibility of about 20 meV was routine and the particular value could be maintained with calibration equipment, applied a few times a year. In the Figure, we find very good news. If we normalize the intensity of the Nion result using a single gain factor, and adjust its EELS axis, using a variable gain and offset, we obtain a very good agreement for the *shape* of the Si edge obtained in the two machines. This is extremely gratifying, because there are differences from the x-ray absorption literature in these results, that were puzzling [34]. This comparison verifies that the spatially resolved EELS is a little different from x-ray absorption spectroscopy and needs to be treated with care until we completely understand and can calculate this shape.

In conclusion, we are witnessing a revolution in capability of electron microscopy and spectroscopy, which owes a debt to Ondrej Krivanek for his dedication and interest to push this so strongly over his career. We have moved from systems having a few dozen optical elements to machines now containing hundreds of ultra-stable current sources. Detector technologies have advanced, and internet operation is now possible, if not convenient, and is very likely to be convenient in near future. We still have much to do, but the results are astonishing, in no small way to the credit of Ondrej, who we wish well on this occasion of a Festschrift in his honor.
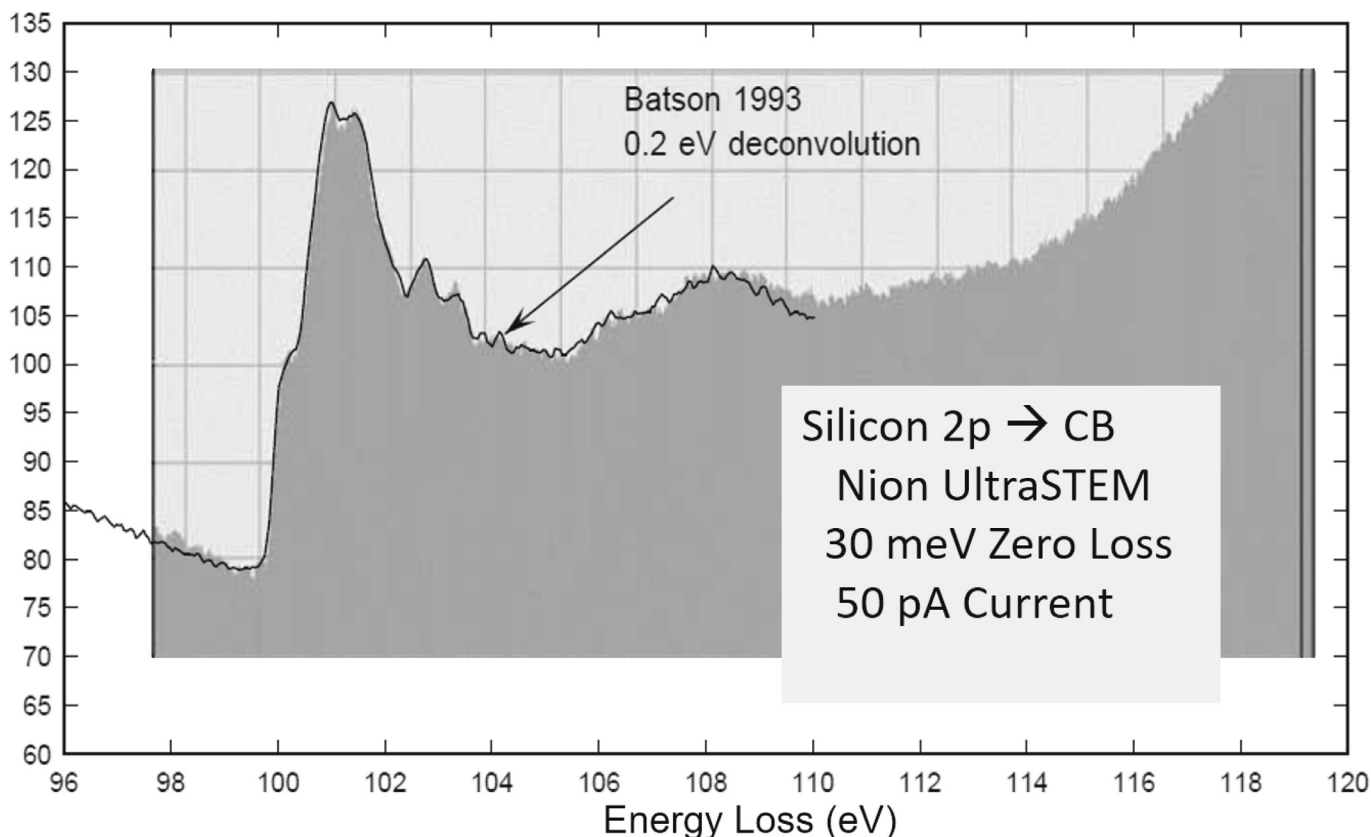
Fig. 10. Comparison of the Si 2p core excitation obtained with the Nion UltraSTEM with the Hermes monochromator, compared with results from the 1990's using the Wien filter spectrometer on the VG Microscopes HB501.

References

[1] P.E. Batson, *Atomic and electronic structure of a dissociated 60◦ misfit dislocation*, Phys. Rev. Lett. 83 (1999) 4409–4412, doi:10.1103/PhysRevLett.83.4409.

[2] P.E. Batson, *Structural and electronic characterization of a dissociated 60◦ dislocation in GeSi*, Phys. Rev. B 61 (2000) 16633–16641, doi:10.1103/PhysRevB.61.16633.

[3] J. Matthews, A. Blakeslee, Defects in epitaxial multilayers, J. Cryst. Growth 27 (1974) 118–125, doi:10.1016/S0022-0248(74)80055-2.

[4] K. Ismail, F.K. LeGoues, K.L. Saenger, M. Arafa, J.O. Chu, P.M. Mooney, B.S. Meyerson, Identification of mobility-limiting scattering mechanism in modulation-doped Si/SiGe heterostructures, Phys. Rev. Lett. 73 (1994) 3447–3450.

[5] L.C. Kimerling, H.J. Leamy, J.R. Patel, The electrical properties of stacking faults and precipitates in heat-treated dislocation-free czochralski silicon, Appl. Phys. Lett. 30 (1977) 217–219.

[6] J.R. Patel, L.C. Kimerling, Dislocation defect states in silicon, J. Phys. Coll. 40 (1979) 67–70.

[7] K. Shum, P.M. Mooney, J.O. Chu, Dislocation-related photoluminescence peak shift due to atomic interdiffusion in SiGe/Si, Appl. Phys. Lett. 71 (1997) 1074–1076.

[8] H. Alexander, Models of dislocation structure, J. Phys. Coll. 40 (1979) 1–6.

[9] A. Olsen, J.C.H. Spence, Distinguishing dissociated glide and shuffle set dislocations in high resolution electron microscopy, Phil. Mag. A 43 (1981) 945–965.

[10] H. Alexander, J.C.H. Spence, D. Shindo, H. Gottschalk, N. Long, Forbidden-reflection lattice imaging for the determination of kink densities on partial dislocations, Phil. Mag. A 53 (1986) 627–643.

[11] V. Higgs, E.C. Lightowlers, C.E. Norman, P. Knightley, Characterisation of dislocations in the presence of transition metal contamination, Mater. Sci. Forum 83–87 (1992) 1309–1314.

[12] J. Weber, Solid State Phenom. 37–38 (1994) 13.

[13] C. Weigel, H. Alexander, J.W. Corbett, Semi-empirical calculations for stacking faults in diamond-type lattices, Phys. Stat. Sol. 71 (1975) 701–706.

[14] L.F. Matheis, J.R. Patel, Electronic stacking-fault states in silicon, Phys. Rev. B 23 (1981) 5384–5396.

[15] M.Y. Chou, M.L. Cohen, S.G. Louie, Theoretical Study of Stacking Faults in Silicon, Phys. Rev. B 32 (1985) 7979–7987.

[16] J.E. Northrup, M.L. Cohen, J.R. Chelikowsky, J. Spence, A. Olsen, *Electronic structure of the unreconstructed 30◦ partial dislocation in silicon*, Phys. Rev. B 24 (1981) 4623–4628.

[17] J.R. Chelikowsky, *30◦ partial dislocations in silicon: absence of electrically active states*, Phys. Rev. Lett. 49 (1982) 1569–1572.

[18] J.R. Chelikowsky, J.C.H. Spence, *Line defects in silicon: the 90◦ partial dislocation*, Phys. Rev. B 30 (1984) 694–701.

[19] J. Bennetto, R.W. Nunes, D. Vanderbilt, *Period doubled structure for the 90◦ partial dislocation in silicon*, Phys. Rev. Lett. 79 (1997) 245–248.

[20] R.W. Nunes, J. Bennetto, D. Vanderbilt, Atomic structure of dislocation kinks in silicon, Phys. Rev. B 57 (1998) 10388–10397.

[21] F. Liu, M. Mostoller, V. Millman, M.F. Chisholm, T. Kaplan, Electronic and elastic properties of edge dislocations in silicon, Phys. Rev. B 51 (1995) 17192–17195.

[22] O.L. Krivanek, N. Dellby, A.J. Spence, R.A. Camps, L.M. Brown, Aberration correction in the STEM, in: Electron Microscopy and Analysis, Institute of Physics, 1997, pp. 35–40.

[23] P.E. Batson, High Resolution Electron Energy Loss Spectrometer for the Scanning Transmis- sion Electron Microscope, Rev. Sci. Inst. 57 (1986) 43–48, doi:10.1063/1.1139116.

[24] P.E. Batson, First results using the nion third-order STEM corrector, in: P. Hawkes (Ed.), Advances in Imaging and Electron Physics, Elsevier, 2008, pp. 163–194.

[25] P.E. Batson, N. Dellby, O.L. Krivanek, Sub-Angstrom resolution using aberration corrected electron optics, Nature 418 (2002) 617–620, doi:10.1038/nature00972.

[26] D.A. Muller, Structure and bonding at the atomic scale by scanning transmission electron microscopy, Nat. Mater. 8 (2009) 263–270, doi:10.1038/nmat2380.

[27] J. Bennetto, R.W. Nunes, D. Vanderbilt, *Period doubled structure for the 90◦ partial dislocation in silicon*, Phys. Rev. Lett. 79 (1997) 245–248.

[28] L. Fabris, Gold-based SERS tags for biomedical imaging, J. Opt. 17 (2015) 114002, doi:10.1088/2040-8978/17/11/114002.

[29] N.I. Cade, T. Ritman-Meer, K.A. Kwakwa, D. Richards, The plasmonic engineering of metal nanoparticles for enhanced fluorescence and Raman scattering, Nanotechnology 20 (2009) 285201 (6pp).

[30] H.A. Atwater, A. Polman, Plasmonics for improved photovoltaic devices, Nat. Mater. 9 (2010) 205–213, doi:10.1038/nmat2629.

[31] R.H. Ritchie, Plasma losses by fast electrons in thin films, Phys. Rev. 106 (1957) 874–881, doi:10.1103/PhysRev.106.874.

[32] C.H. Chen, J. Silcox, Calculations of the electron-energy-loss probability in thin uniaxial crystals at oblique incidence, Phys. Rev. B 20 (1979) 3605–3614, doi:10.1103/PhysRevB.20.3605.

[33] R. Geick, C.H. Perry, G. Rupprecht, Normal modes in hexagonal boron nitride, Phys. Rev. 146 (1966) 543–547, doi:10.1103/PhysRev.146.543.

[34] P.E. Batson, Distortion of the core exciton by the swift electron in electron energy loss scattering, Phys. Rev. B 47 (1993) 6898–6910, doi:10.1103/PhysRevB.47.6898.

[35] J.R. Patel, L.R. Testardi, P.E. Freeland, Electronic effects on dislocation velocities in heavily doped silicon, Phys. Rev. B 13 (1976) 3548–3557.

[36] P.E. Batson, High resolution electron energy loss spectrometer for the scanning transmission electron microscope, Rev. Sci. Inst. 57 (1986) 43–48, doi:10.1063/1.1139116.